ROSAT X-Ray Observations of the 2A 0335+096 Cluster of Galaxies

Jimmy A. Irwin – University of Virginia
Craig L. Sarazin – University of Virginia

Citation of published version:

Irwin, J., Sarazin, C. (1995): ROSAT X-Ray Observations of the 2A 0335+096 Cluster of Galaxies. *The Astrophysical Journal*, vol. 455. DOI: 10.1086/176599

THE ASTROPHYSICAL JOURNAL, 455:497–507, 1995 December 20

ROSAT X-RAY OBSERVATIONS OF THE 2A 0335+096 CLUSTER OF GALAXIES

JIMMY A. IRWIN AND CRAIG L. SARAZIN
Department of Astronomy, University of Virginia, P.O. Box 3818, Charlottesville, VA 22903-0818;
jai7e, cls7i@virginia.edu
Received 1995 January 18; accepted 1995 June 23

ABSTRACT

The 2A 0335+096 cluster of galaxies was observed in X-rays with the Position Sensitive Proportional Counter (PSPC) and the High Resolution Imager (HRI) on *ROSAT*. Spatially resolved X-ray spectra show a decrease in the ambient temperature of the X-ray emitting gas in the inner regions of the cluster, indicative of a cooling flow. The spectra also confirm the presence of an absorbing column density in excess of the measured Galactic value toward the cooling flow region, which must be intrinsic to the cluster. The mass of this absorbing matter is $7.4 \times 10^{11}\ M_\odot$ within 170 kpc of the center of the cluster. A deprojection of the surface brightness profile combined with the observed temperature profile yields electron density, gas and gravitational mass, and mass deposition rate profiles. Within 1.2 Mpc the total gravitating mass is $1.9 \times 10^{14}\ M_\odot$. A cooling rate of $400^{+90}_{-65}\ M_\odot\ \mathrm{yr}^{-1}$ is found within the cooling radius of 166^{+28}_{-18} kpc. This value is consistent with the cooling rate obtained by fitting a cooling flow model to the spectrum of the central 166 kpc. Although the cooling rate is proportional to radius for the inner 60 kpc, it is essentially constant beyond this point, which suggests that the gas cools homogeneously in this region. A similar result was found for the NGC 5044 group of galaxies by David et al. (1994). This disagrees with earlier observations of other clusters, which suggested that the gas within the entire cooling flow region was inhomogeneous.

Subject headings: cooling flows — galaxies: clusters: individual (2A 0335+096) — intergalactic medium — X-rays: galaxies

1. INTRODUCTION

Observations of clusters of galaxies over the last two decades have shown that they contain large quantities ($\sim 10^{14}\ M_\odot$) of hot, X-ray emitting gas that can extend out beyond 3 Mpc from the center of the cluster. The discovery of Fe–K emission lines within clusters (Mitchell et al. 1976; Serlemitsos et al. 1977) showed the gas to be metal enriched, with a heavy element abundance on the order of 40% of the solar value. These studies have also confirmed that the X-ray emission mechanism is thermal bremsstrahlung and line emission from a hot diffuse plasma.

The central electron densities inferred from imaging studies in many clusters imply a radiative cooling time much less than the probable age of the cluster. As the gas cools, mass must flow in from larger radii to maintain pressure equilibrium, which creates a cooling flow (a review of cooling flows is presented in Fabian 1994). The X-ray emission in these clusters is invariably centered on a D or cD galaxy. Cooling flow clusters are also characterized by a central spike in the surface brightness profile, as the density rises very steeply in the inner region of the cluster. X-ray spectra of cooling flow regions confirm the presence of a low-temperature component of the gas in this region and yield cooling rates in agreement with imaging studies.

What happens to the gas after it cools below X-ray emitting temperatures remains a mystery. A typical cooling rate of $\sim 100\ M_\odot\ \mathrm{yr}^{-1}$ will deposit $\sim 10^{12}\ M_\odot$ of material over the lifetime of the cluster. It has been suggested (see, e.g., Fabian, Nulsen, & Canizares 1982; Sarazin & O'Connell 1983; O'Connell & McNamara 1989) that the cooled gas forms stars, although the initial mass function (IMF) of the cooling flow must be significantly different from the local IMF to account for the weakness of the blue light characteristic of massive stars in all but the very center of the cooling flow (Romanishin & Hintzen 1988). Alternatively, the cooled gas may be in the form of cold, dense clouds. White et al. (1991) have demonstrated the presence in 12 clusters of excess X-ray absorption above that due to Galactic absorption. The inferred mass of the absorbing material (presumably in the form of cold gas clouds) is 3×10^{11}–$10^{12}\ M_\odot$. However, there does not seem to be a clear relation between the mass of the absorbing material and the cooling rate of the cluster.

X-ray observations of clusters of galaxies provide a convenient method of determining the total gravitational mass in clusters with poorly determined galaxy velocity distributions. The amount and form of dark matter (the difference between the gravitational mass and the mass in gas and stars) in a cluster has important cosmological implications. Previous studies (Briel, Henry, & Böhringer 1992; David et al. 1994) have shown that the baryonic fraction of the mass in clusters is several times larger than that allowed by big bang nucleosynthesis in an $\Omega = 1$ universe (White et al. 1993).

Previous X-ray satellites have had insufficient spectral and spatial resolution to determine accurately the temperature profile of clusters, a necessary ingredient in determining the gravitational mass profile and the profiles of other relevant cluster properties. Either a single global temperature for the cluster was used, or a gravitational potential profile was assumed. However, the improved spectral resolution of the *ROSAT* Position Sensitive Proportional Counter (PSPC) permits for the first time the determination of the temperature profile, which can directly be used in the analysis of the cluster. Combined with the high spatial resolution of the High Resolution Imager (HRI), a detailed profile of cluster properties can be obtained.

At a redshift of $z = 0.035$, 2A 0335+096 has many of the most interesting properties of cooling flow clusters. It has evidence of low-energy X-ray and optical line emission, soft X-ray

absorption, a rather large cooling rate, and filamentary X-ray structure in the central regions. With a global temperature of 3.1 keV (White et al. 1991), the 0.1–2.48 keV bandpass of *ROSAT* should allow for an accurate measurement of the variation of temperature. Previous studies have derived cooling rates in the cluster, which ranged from 14–262 $M_\odot$ yr^{-1} (Singh, Westergaard, & Schnopper 1988; White et al. 1991; Sarazin, O'Connell, & McNamara 1992).

This paper is organized as follows. In § 2, we describe the observations made by the PSPC and HRI, and in § 3, we discuss the global appearance of the cluster and other sources in the field of view. The spectral and spatial analyses are summarized in §§ 4 and 5, respectively. In § 6, we describe the deprojection of the surface brightness profile and the resulting density and mass profiles. The cooling rate profile is presented in § 7. In § 8, we discuss the implications of our analysis, and our conclusions are reviewed in § 9.

2. X-RAY OBSERVATIONS

The cluster 2A 0335+096 was observed with the PSPC for 8185 s over the period 1991 February 25 to 1992 August 25. Periods of high background due to charged particles were removed by filtering the original image such that all time intervals with a Master Veto Rate above 170 counts s^{-1} were excluded, resulting in an effective exposure of 7678 s (see Plucinsky et al. 1993 for a description of the charged particle rejection efficiency of the PSPC). The cluster was also observed with the HRI over the period 1991 February 10–14 for 14,012 s. Periods of high background near the beginning and end of the observation intervals were removed, leaving 12,959 s of useful observation time. The spectral analysis in this study was performed using the XSPEC package, and the spatial analysis was performed in part using the PROS package within IRAF. We assume a Hubble constant of $H_0 = 50$ km s^{-1} Mpc^{-1} and a cosmological deceleration parameter of $q_0 = 0.5$ throughout this paper. At a redshift of $z = 0.035$ the cluster is at an angular diameter distance of 198 Mpc, and 1′ corresponds to 57.5 kpc.

3. GLOBAL PROPERTIES AND OTHER SOURCES

Figure 1 shows a contour plot of the PSPC image after smoothing using an adaptive kernel density estimation method (Silverman 1986; Huang & Sarazin 1996), which varies the smoothing length according to the local surface brightness distribution. Bright, high-density regions are smoothed very little in order to preserve structure while faint, low-density regions are smoothed to a greater extent to remove the grainy appearance associated with photon noise. A constant signal-to-noise ratio of 5 was used to determine the smoothing length of the Gaussian beam. One pixel corresponds to 7.″5. The contours appear smooth and slightly elliptical. Although the inner isophotes center on the position of the D galaxy, the outer isophotes seem to center on a point slightly northwest of the D galaxy. The HRI image of the cooling flow region, a *V*-band CCD image, and a discussion of the central region is presented in Sarazin et al. (1992). All point sources were removed before the diffuse cluster emission was analyzed. The centroid of the X-ray emission lies very close to the optical center of the central D galaxy of the cluster at R.A. = $3^h38^m40^s.5$ and Decl. = 9°58′11.″6 (J2000; Sarazin et al. 1992).

A number of individual X-ray sources were also detected in the PSPC and HRI observations using the standard detection algorithms in PROS. These detection algorithms are often con-

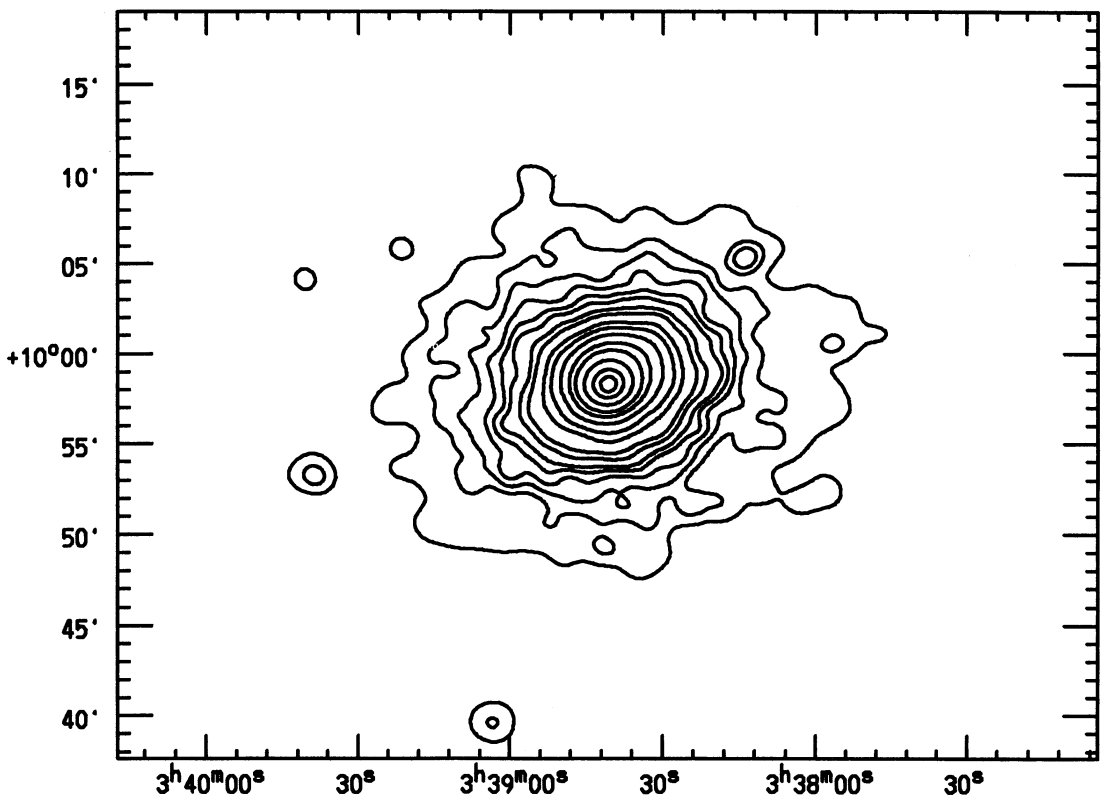

FIG. 1.—Contour plot of the *ROSAT* PSPC X-ray image in the 0.42–2.48 keV band after adaptive kernel smoothing. A constant S/N of 5 was used to determine the smoothing length. The coordinates are R.A. and Decl. (J2000). The contour levels are 0.1, 0.2, 0.3, 0.4, 0.5, 0.6, 0.8, 1, 1.5, 2, 3, 5, 8, 16, 30, and 42 counts per pixel (7.″5). The source 9.′6 to the northwest of the cluster is a Narrow Angle Tail radio galaxy.

fused by extended X-ray sources such as clusters of galaxies, and "detect" a large number of sources associated with gradients in the cluster X-ray surface brightness. We have examined the positions of the detected sources, and rejected any that did not correspond to significant enhancements in the local surface brightness. (A few of the remaining sources were extended and diffuse, and may be fluctuations in the cluster X-ray surface brightness; these are indicated by the notation "Fluct?" below.) A list of sources from the PSPC and HRI is given in Table 1. The first column gives the source number, while the second and third columns give the source position. The count rate and *ROSAT* instrument are given in the fourth and fifth columns. Some of the sources have very uncertain fluxes because of either their proximity to a rib structure or their distance from the center of the observing field. Note that only two sources are given from the HRI observation. One of these (source 8) was also detected with the PSPC. Many of the PSPC sources are outside the field of view of the HRI. The distance of the source from the center of the observing field is given in the sixth column.

The last column gives comments or information on the identification of the sources. We sought identifications by comparing the positions of the sources to *Hubble Space Telescope* Guide Star Catalog (GSC) positions (Lasker et al. 1988), to the digitized *Hubble Space Telescope* Guide Star images (kindly provided by Ralph Bohlin), to the radio observations of Sarazin, Baum, & O'Dea (1995), to the positions of cluster galaxies, and to a variety of astronomical catalogs. Seven sources are identified with optical objects in the Guide Star Catalog; these are indicated with "GSC" is Table 1, except for the two sources (8 and 22) that had more detailed information from other sources. Several other sources coincide with fainter optical features; these are indicated with the notation "Faint opt?" in the table. We also generated random lists of X-ray source positions to compare to the optical objects, and we found that the identifications with bright optical sources are probably real (they are unlikely to occur by chance), while the identifications with fainter objects may not be real. Source 19 is near the eighth brightest cluster galaxy. The position of source 21 is near a radio source (Sarazin et al. 1995) and a faint spiral galaxy.

The positions of the sources with bright optical identifications and good optical positions were used to check and improve the positions on the *ROSAT* PSPC image. These improved positions were particularly important for comparing the X-ray positions to those of the radio sources in the cluster (Sarazin et al. 1995).

Two sources merit additional comments. Source 22 agrees very well with the position of the G star HD 22670. The colors of this star suggest that it is not very distant or highly reddened. The observed X-ray to optical flux ratio of this object would place it near the median of G stars detected in X-rays with the *Einstein Observatory* (see, e.g., Vaiana 1990). Thus, it appears likely that this identification is correct.

Source 8 is identified with the second brightest elliptical galaxy in the cluster, which hosts a luminous and extremely long Narrow Angle Tail (NAT) radio galaxy (seen as the bright source 9'.6 northwest of the center of the cluster in Fig. 1). Source 8 was detected with both the PSPC and the HRI. The X-ray source is discussed in considerable detail in Sarazin et al. (1995). It appears to be unresolved (although it is difficult to determine this given the cluster background), and is somewhat brighter than X-ray bright normal ellipticals of the same optical luminosity. Sarazin et al. suggest that the X-ray source is associated with the active nucleus in the radio galaxy.

4. SPECTRAL ANALYSIS

In order to determine the temperature profile of the cluster, spectral fits were performed on five annular regions centered on the position of the nucleus of the central D galaxy of the

TABLE 1

OTHER X-RAY SOURCES

Source Number	R.A. (J2000)	Decl. (J2000)	Count Rate (10^{-3} s^{-1})	Instrument	D	ID or Comment
1	$3^h37^m23^s.8$	10°43'35"	22.6[a]	PSPC	49.0	
2	3 39 17.1	10 38 00	15.9[a]	PSPC	40.8	Faint opt?
3	3 38 28.2	10 25 38	13.3[a]	PSPC	27.6	Optical ID, GSC V = 12.9
4	3 38 48.8	10 22 33	8.8[a]	PSPC	24.4	
5	3 38 18.7	10 20 15	21.9[a]	PSPC	22.7	Optical ID, GSC V = 11.0
6	3 35 51.6	10 17 34	12.8[a]	PSPC	45.6	Close to rib, GSC V = 15.2?
7	3 39 18.8	10 13 53	3.5 ± 0.9	PSPC	18.3	
8	3 38 14.0	10 05 05	7.7 ± 1.2	PSPC	9.5	Galaxy, NAT Radio Source
	3 38 14.2	10 05 12	1.3 ± 0.3	HRI	9.6	
9	3 37 56.0	10 00 24	3.0 ± 0.7	PSPC	11.2	Faint opt?
10	3 37 59.1	9 57 34	5.3 ± 1.1	PSPC	10.3	Faint opt? Fluct?
11	3 38 09.5	9 55 05	9.1 ± 1.4	PSPC	8.3	Fluct?
12	3 39 01.1	9 53 25	1.1 ± 0.3	HRI	7.0	Faint opt?
13	3 39 39.7	9 52 46	10.4 ± 1.5	PSPC	15.3	Faint opt?
14	3 37 57.9	9 52 06	1.8 ± 0.6	PSPC	12.2	Fluct?
15	3 38 25.1	9 51 35	8.0 ± 1.3	PSPC	7.7	
16	3 38 03.3	9 51 34	2.2 ± 0.7	PSPC	11.4	Faint opt? Fluct?
17	3 38 18.9	9 51 26	2.2 ± 0.7	PSPC	8.7	
18	3 38 42.3	9 49 10	4.8 ± 1.0	PSPC	9.0	Fluct?
19	3 38 48.4	9 48 56	1.8 ± 0.6	PSPC	9.4	Galaxy G8?
20	3 38 32.8	9 48 50	1.5 ± 0.5	PSPC	9.6	Optical ID? GSC V = 14.6
21	3 38 56.6	9 42 23	3.0 ± 0.8	PSPC	16.2	Faint Opt? Galaxy? Radio?
22	3 39 04.5	9 39 09	17.4 ± 2.1	PSPC	19.8	Optical ID, HD22670 V = 9.0
23	3 38 35.3	9 33 24	14.7[a]	PSPC	24.8	
24	3 39 11.7	9 27 52	23.4[a]	PSPC	31.2	Optical ID, GSC V = 12.4

[a] These sources have very uncertain fluxes because of either their proximity to a rib structure or their distance from the center of the observing field.

cluster. The annuli were chosen such that each was larger than the joint XRT and PSPC point spread function (Hasinger et al. 1992) and contained enough counts to determine accurately the temperature of the annulus. The outermost annulus extends out to the inside of the rib support structure (18′). The angular extent and number of X-ray counts of each of the five annuli are listed in Table 2.

The spectra of the annuli were corrected for vignetting and particle background according to the Plucinsky et al. (1993) parameterization of the average Master Veto Rate of the observation. A background spectrum, extracted from an annulus of 30′–35′ (1725–2010 kpc) and corrected for vignetting, was scaled to and subtracted from each source spectrum. The energy channels were rebinned to the standard 34 channel PROS format and all channels below 0.2 keV (pulse invariant [PI] channels <20) were ignored in the fit, since the equations governing the charged particle parameterization are not applicable in that region of the spectrum. The remaining 29 energy channels were used in the spectral fit.

As a first attempt at fitting a spectral model to the data, a Raymond-Smith thermal plasma model (Raymond & Smith 1977) with a photoelectric absorption component (Morrison & McCammon 1983) fixed at the Galactic neutral hydrogen column density value ($N_{\rm H} = 1.71 \times 10^{21}$ cm^{-2}; Stark et al. 1992) was used (model 1). The abundance of the Raymond-Smith component was fixed at 40% of solar, the value derived from an *EXOSAT* study of the cluster (Singh, Westergaard, & Schnopper 1986). A chi-squared minimization routine within XSPEC was utilized in order to determine the acceptability of the fit. The only free parameters were the temperature and normalization of the Raymond-Smith component, leaving 27 degrees of freedom for the fit. Although the model gave acceptable fits for the outer two annuli, it was unsuccessful in fitting the inner annuli (see Table 2). Allowing the abundance to vary improved the fits somewhat but not to a statistically acceptable level.

An additional variable absorption component due to a cold absorber with a covering factor of unity at the redshift of the cluster was then added to the model (model 2) and the abundance was once again fixed at 40%. The fits were markedly improved by the addition of this component. The best-fitting temperature, excess column density, and minimum χ^2-values for each annulus are summarized in Table 2. The uncertainties represent the 90% confidence ranges for one interesting parameter ($\Delta\chi^2_{\rm min} = 2.71$). The fact that extra absorption that is intrinsic to the cluster was found is not surprising in light of recent findings of the same phenomenon by several authors (White et al. 1991; Allen et al. 1993; Allen & Fabian 1994). Still, an acceptable fit was not found for the innermost annulus, which most likely contains a temperature gradient and is, therefore, unlikely to be well-modeled by a single-temperature component. Since previous studies indicate that this cluster possesses a significant cooling flow, a cooling flow component (Mushotzky & Szymkowiak 1988) was added to the model (model 3) for each annulus with the upper temperature from which the gas cools set equal to the temperature of the Raymond-Smith component. The Galactic absorption was once again fixed at the measured value and the variable absorption component was allowed to act on both the cooling flow and Raymond-Smith components. The gas in the cooling flow was assumed to cool to zero, and the cooling rate, $\dot{M}$, was left as a free parameter. A cooling flow component was not required at all in the outer two annuli. There was only a marginal improvement in the fits of the second and third annuli, at the expense of tremendously expanding the error bars of the temperature. A statistically acceptable fit was obtained for the innermost annulus using this model ($\chi^2 = 27.7$ for 25 degrees of freedom). The best-fitting temperature, excess column density, cooling rate, and minimum χ^2-values for this model for each annulus are summarized in Table 2.

We investigated the possibility that the excess absorption was an artifact of either assuming an incorrect metallicity for the gas or errors in the assumed plasma code emissivities around 1 keV. By varying the abundance in the fits between 0.2–0.55 (the 99% confidence levels for the metallicity from the *EXOSAT* study; Singh, Westergaard, & Schnopper 1986), the amount of excess absorption decreased by less than 20% in all five annular bins. We also fitted the spectra using a revised version of the Mewe and Gronenschild (MG) thermal plasma model (Kaastra 1992). This model differs most significantly from the Raymond-Smith model in the emission lines emissivities around 1 keV. The results from using the MG model were very similar to those obtained with the Raymond-Smith model. Therefore, it seems unlikely that the need for excess absorption is a result of uncertainties in the metallicity or plasma code emissivities.

Further evidence that excess absorption is required to model the spectra of the cooling core of this cluster is presented in Figures 2*a*–2*d*. In § 6 below, we show that the cooling radius (the position at which the cooling time equals the age of the cluster) is approximately $r_c \approx 166$ kpc (2.′9). The spectrum of this region (the inner 166 kpc) and the best-fit single thermal component model (model 1) with contributions to χ^2 for each energy bin plotted beneath are shown in Figure 2*a*. Clearly, the model overestimates the amount of soft X-ray emission

TABLE 2

SPECTRAL FITS IN ANNULI

		MODEL 1 (27 DOF) SINGLE-TEMPERATURE NO INTRINSIC ABSORPTION		MODEL 2 (26 DOF) SINGLE-TEMPERATURE INTRINSIC ABSORPTION			MODEL 3 (25 DOF) COOLING FLOW + SINGLE-TEMPERATURE INTRINSIC ABSORPTION			
ANNULUS	COUNTS	kT (keV)	χ^2	kT (keV)	$\Delta N_{\rm H}$ (10^{21} cm^{-2})	χ^2	kT (keV)	$\Delta N_{\rm H}$ (10^{21} cm^{-2})	$\dot{M}$ ($M_\odot$ yr^{-1})	χ^2
0′–1.′5.....	9652	1.51	101.1	1.38	0.70	38.9	$1.52^{+0.18}_{-0.13}$	$1.22^{+0.40}_{-0.33}$	251^{+153}_{-118}	27.7
1.5–3	4231	7.25	69.6	$2.73^{+0.84}_{-0.53}$	$0.90^{+0.26}_{-0.24}$	29.3	3.28	1.22	51.5	26.7
3–6.....	3384	6.99	39.7	$3.59^{+1.97}_{-0.97}$	$0.55^{+0.30}_{-0.29}$	29.5	5.64	0.86	42.4	27.3
6–9	1480	3.68	31.0	$2.46^{+1.77}_{-0.69}$	$0.59^{+0.50}_{-0.44}$	26.1	2.46	0.59	0.02	26.1
9–18.....	1594	2.49	28.0	$2.49^{+2.14}_{-0.82}$	$0^{+0.61}_{-0.00}$	28.0	2.45	0.00	0.00	28.0

NOTE.—Error bars represent the 90% confidence ranges for one interesting parameter ($\Delta\chi^2_{\rm min} = 2.71$). Error bars are listed only for the adopted model spectrum of that annulus.

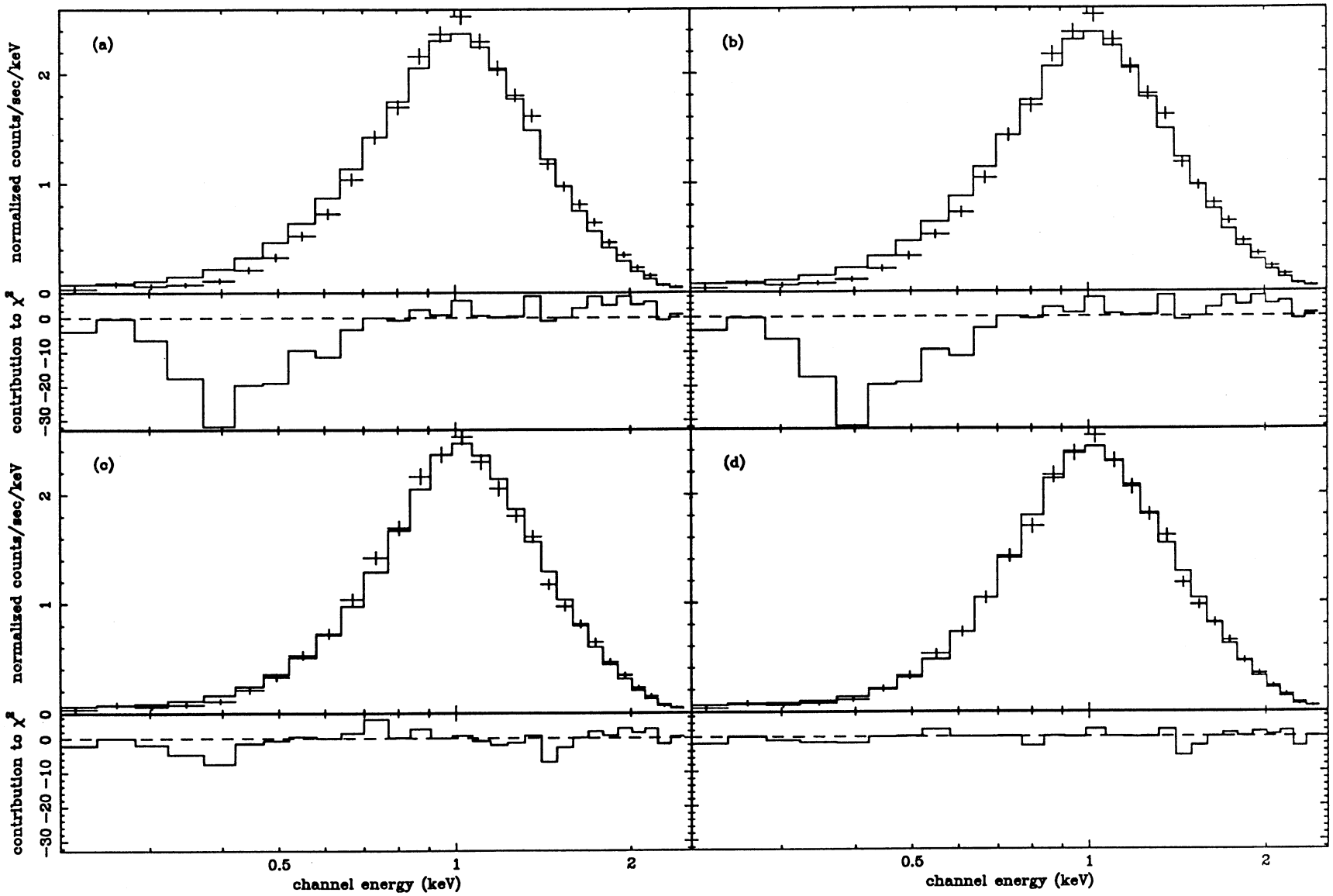

FIG. 2.—Best-fit models for the PSPC spectrum of the cooling flow region ($r \leq r_c = 166$ kpc) assuming: (*a*) Raymond-Smith thermal spectrum with Galactic absorption; (*b*) a cooling flow component added to a Raymond-Smith thermal spectrum with Galactic absorption; (*c*) a variable intrinsic absorption component superposed on a Raymond-Smith thermal spectrum with Galactic absorption model; and (*d*) a cooling flow component and variable intrinsic absorption component added to a Raymond-Smith thermal component with Galactic absorption model. The contributions of each energy bin to the χ^2 value multiplied by the sign of the residual are shown in the lower window of each plot.

($\chi^2 = 169.6$ for 27 degrees of freedom). The hard end of the spectrum is also poorly fit. The addition of a cooling flow component (Fig. 2*b*) does little to improve the fit, since cooling gas increases the amount of soft X-ray emission of the model. However, if the cooling flow component is removed and a variable absorption component is added (model 2), the resultant spectral model fits the data much better (Fig. 2*c*). The addition of a cooling flow component (model 3) then improves the fit even more ($\chi^2 = 31.88$ for 25 degrees of freedom; Fig. 2*d*). The deficit of soft X-ray emission is now accounted for with this model. (It is likely that the temperature gradient in this region [Table 2] results in the poorer fit to a single model for the entire cooling flow region.) The cooling rate for this model is $367^{+166}_{-146}\ M_\odot\ \mathrm{yr}^{-1}$, in good agreement with the value of 400 $M_\odot$ yr^{-1} derived from the deprojection analysis (§ 6 below). We note that our derived value for the cooling rate is larger than previous studies have indicated, which have ranged from 14–262 $M_\odot$ yr^{-1} (Singh, Westergaard, & Schnopper 1988; White et al. 1991; Sarazin et al. 1992).

Figures 3 and 4 show the radial profiles of the temperature and excess column density. Within the error bars the cluster is isothermal throughout the outer four annuli. The innermost annulus clearly contains gas at a lower temperature than the rest of the cluster, a strong indication that a cooling flow is present in this cluster. The amount of excess column density increases with decreasing radius and becomes comparable to the Galactic value within 170 kpc of the center of the cluster. The implications of this radial trend will be discussed in § 8.

Since a continuous temperature profile is required for the deprojection technique described in § 6, a simple function was fit to the five annular temperature values (as shown in Fig. 3). Since the gas is nearly isothermal in all but the core of the cluster, a single spectral fit was performed on a region extending from 122 kpc to the inside of the rib support structure with

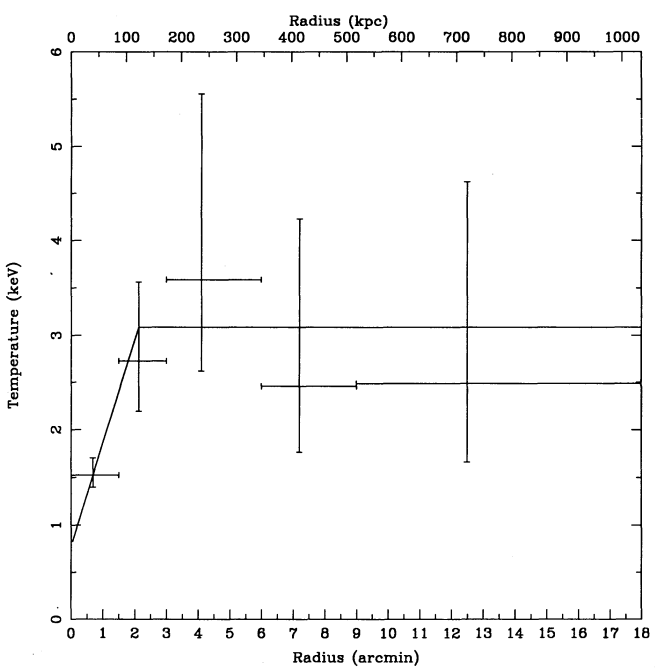

FIG. 3.—Temperature profile of 2A 0335+096 derived from the PSPC spectral analysis. Error bars are the 90% confidence regions for a single interesting parameter. The solid line represents the temperature function used in the deprojection of the surface brightness profile.

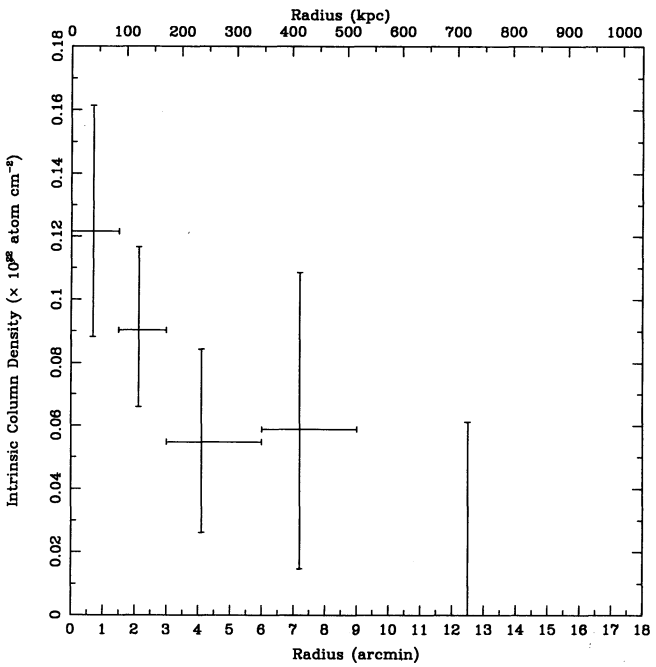

FIG. 4.—Excess absorption profile for the cluster derived from the PSPC spectral analysis. The error bars are the 90% confidence regions for a single interesting parameter.

the same model that was used on the outer four annuli (model 2). An acceptable fit was obtained using this model ($\chi^2 = 24.7$ for 26 degrees of freedom) with a temperature of $3.1^{+0.9}_{-0.6}$ keV, in good agreement with the global value of 2.9 ± 0.3 keV derived from the *EXOSAT* ME (Singh et al. 1986) and 3.1 keV derived from the *Einstein* Solid State Spectrometer (SSS) (White et al. 1991). The temperature profile then decreased linearly inward from 122 kpc to the center, passing through the temperature value of the innermost annulus at 40 kpc (40 and 122 kpc are the points within the first and second annuli, respectively, which divide the number of counts in that annulus in half). Although this function represents the *projected* temperature profile, Allen & Fabian (1994) have demonstrated that projection effects do not lead to a significant overestimation of the temperature of the inner annuli due to the superposition of the hotter isothermal gas in the outer regions of the cluster.

5. SPATIAL ANALYSIS

We first consider the shape of the cluster X-ray distribution. We determined this by fitting elliptical isophotes to the cluster X-ray surface brightness. Elliptical isophotes centered on the central D galaxy were fitted to both the HRI and PSPC images using an algorithm developed by Jedrzejewski (1987). Given an initial estimate of the ellipticity and position angle of the major axis of the ellipse (measured from north through east), the routine ELLIPSE within IRAF calculates the best-fit values for these two parameters for a given value of the semi-major axis. As the length of the semi-major axis is increased, a profile of the variation of ellipticity and position angle with radius is obtained. This procedure was carried out on both the HRI and PSPC after blocking down each image to a 512 × 512 array (8″ and 15″ pixels for the HRI and PSPC images, respectively). Such a large blocking factor was needed in order to ensure that

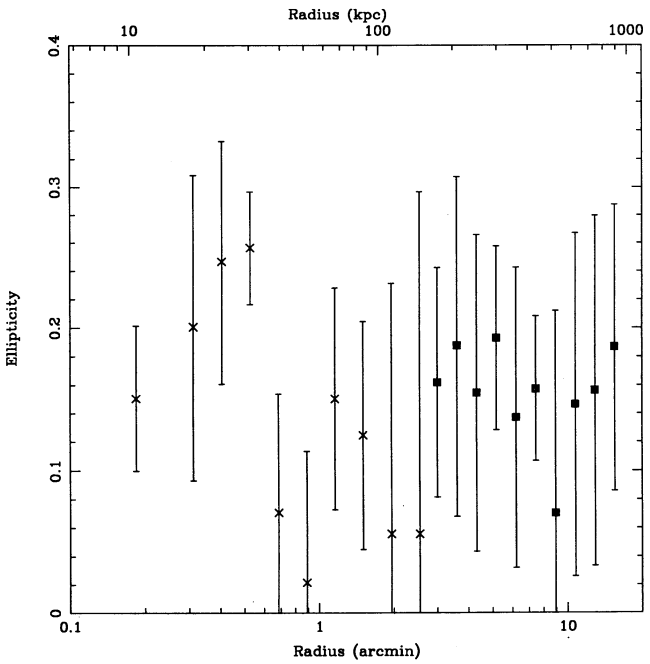

FIG. 5.—Variation of ellipticity with radius for the inner 16′. The crosses are the HRI data, while the filled boxes refer to the PSPC image.

the number of counts per pixel was large enough to determine accurately the variation in ellipticity and position angle out to 3′ for the HRI and out to 16′ for the PSPC.

The results of the fitting process are shown in Figures 5 and 6. Note that the ellipticity is always less than 0.3, with an average of about 0.2, and the position angle is approximately a constant. Large errors in the position angle occur where either the surface brightness is low, or where the ellipticity is nearly

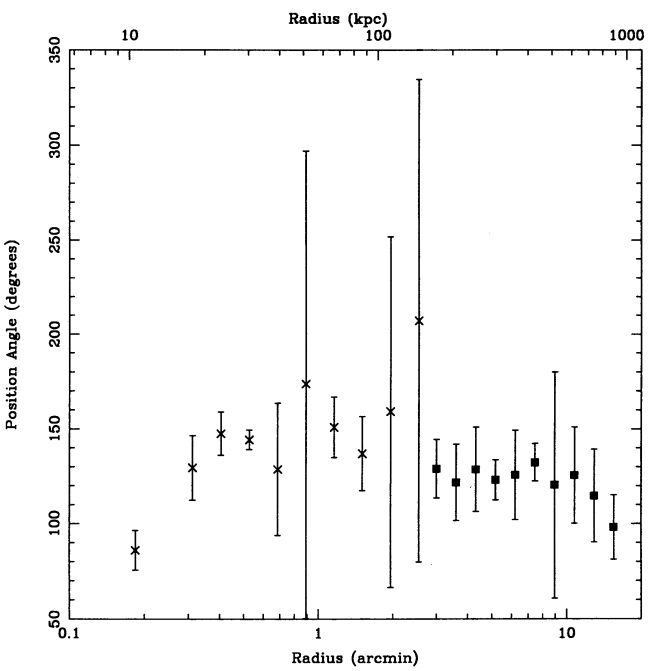

FIG. 6.—Variation of position angle with radius for the inner 16′. The crosses are the HRI data, while the filled boxes refer to the PSPC image.

zero. At the smallest radii, the orientation is affected by the central X-ray bar (Sarazin et al. 1992). White et al. (1994) have demonstrated that for Abell 478, for which the ellipticity of the cluster is about 0.2, the assumption of circular symmetry does not significantly affect their results. By dividing the cluster into four sectors and performing their analysis on each sector independently, they were able to show that the averages of the gas mass, cooling radius, and mass deposition rate values from the four sectors were consistent with the values obtained by performing the analysis on the cluster as a whole. Since 2A 0335+096 has an ellipticity of less than 0.2, we shall proceed under the assumption of circular symmetry.

For the purposes of deriving the profile of the X-ray surface brightness, the PSPC image was filtered to exclude all energy channels below 0.42 keV (PI channels <42). Since most of the background in the PSPC is composed of low-energy events (particle background is rejected at a very high efficiency), eliminating these soft channels reduced the background by 75% while only reducing the source counts by a few percent. The counts in annular bins centered on the central D galaxy were summed and then corrected for vignetting. A background annulus between 30′–40′ corrected for vignetting was normalized to and subtracted from each bin. A profile was also generated for the HRI using a background region of 10′–15′. Since the background in the HRI primarily results from charged particles and residual radioactivity produced within the detector, the background-subtraction process of the HRI differs from that of the PSPC. After subtracting off the unvignetted charged particle and internally produced background from the source bins, the remaining X-ray background (which comprises about 20% of the total background; David et al. 1992) was corrected for vignetting and subsequently normalized to and subtracted from each source bin.

In order to utilize the superior spatial resolution of the HRI and the superior sensitivity of the PSPC, the two profiles were joined at 3′. The best-fit spectrum in the region 3′–6′ (given in Table 2) gave energy fluxes for the HRI and PSPC that agreed to within 4%. The slopes of the radial profiles for the HRI and PSPC were also equal in this region. The HRI counts were multiplied by 2.66 to normalize them to the PSPC counts. Figure 7 shows the radial profiles of the combined HRI+PSPC data (*solid line*) and the PSPC alone (*dotted line*). The superior resolution of the HRI becomes apparent within 0.6 (35 kpc) of the center of the profile.

Assuming a thermal spectrum of 3.1 keV, a Galactic column density of $N_H = 1.71 \times 10^{21}$ cm^{-2} and an intrinsic absorption column density of $\Delta N_H = 5.2 \times 10^{20}$ cm^{-2} (the best-fit values of model 2 for the entire cluster except the innermost annulus), the counts to energy ratio was calculated and the surface brightness profile was obtained. Figure 8 shows the X-ray surface brightness profile in the photon energy band (0.42–2.48 keV) with 1 σ errors. The inner point is affected by the spatial resolution of the HRI. The profile can be traced out to a distance of 1.6 Mpc.

6. DEPROJECTION AND MASS DISTRIBUTIONS

Assuming that the X-ray emission is spherically symmetric, we can deproject the surface brightness profile to yield the emissivity profile. The basic technique for doing this was developed by Fabian et al. (1981), and has been applied to a large number of *Einstein* observations of clusters (Arnaud 1988). More recently, similar techniques were developed for *ROSAT* images (see, e.g., Allen et al. 1993), making use of the enhanced

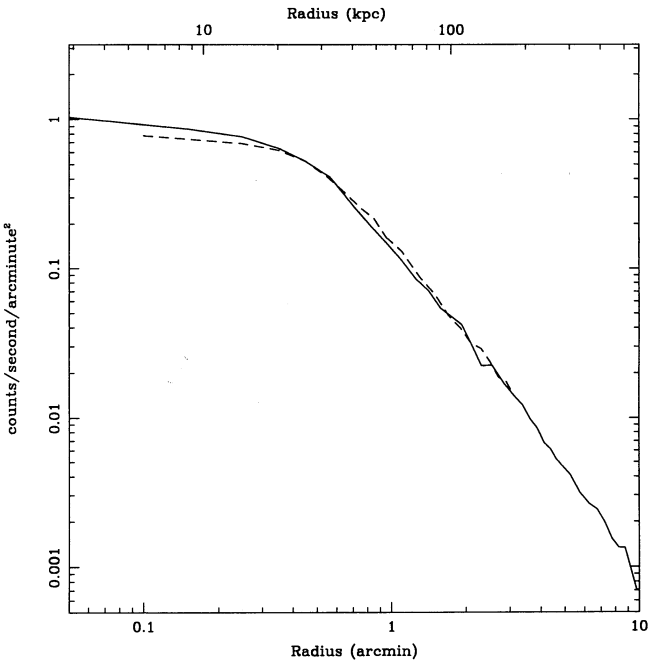

FIG. 7.—Radial profile of the X-ray count rate of 2A 0335+096 for the PSPC alone (*dotted line*) and for the combined PSPC + HRI data (*solid line*).

spectral resolution of the PSPC. By assuming that all the emission in the outermost bin j of projected radius b is not contaminated by photons originating from a true radius $r > b$ projected into our line of sight, the emissivity in that bin can easily be calculated. Then the surface brightness in bin $j - 1$ can be corrected for projection effects from bin j to determine its emissivity. The emissivity in bin $j - 2$ can be calculated after correcting for projection effects from bins j and $j - 1$. This iterative process is continued until the innermost bin is reached. One might suspect that the emissivity profile is dependent on the value adopted for the outermost bin. However, we find that varying the emissivity value for the outermost bin by as much as an order of magnitude has a negligible effect on the values derived within 700 kpc of the center. Hence, the assumption that the outermost bin is not contaminated from projection effects is not critical to our analysis.

The electron density profile can readily be derived from the emissivity profile if the temperature profile is known. The great advantage of *ROSAT* PSPC observations for this purpose is that the enhanced spectral resolution allows one to directly determine the temperature profile (see, e.g., Allen et al. 1993). However, in the past temperature profiles were not directly available due to the limited spectral and spatial resolution of X-ray satellites such as *EXOSAT* and *Einstein*.

With the temperature profile from § 4, the electron density profile, $n_e(r)$, can be derived from the emissivity profile, $\epsilon_X(r)$, through the relation

$$\epsilon_X(r) = \Lambda_X[T(r)]n_e^2(r)\,, \tag{1}$$

where $\Lambda_X(T)$ is the X-ray emissivity coefficient, and $T(r)$ is the gas temperature at a radius r. The profile of the electron density of the gas is shown in Figure 9. The gas mass profile follows easily from the integral of the electron density profile.

The gas pressure follows from the ideal gas law

$$P = \frac{\rho kT}{\mu m_H}\,, \tag{2}$$

where ρ and μ are the gas mass density and molecular weight, respectively. If hydrostatic equilibrium is assumed and only gas pressure contributes to the support of the gas, the total gravi-

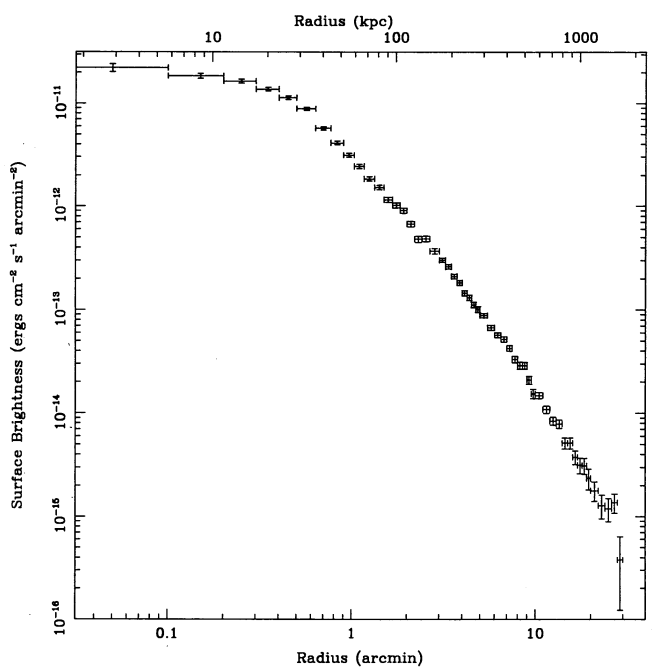

FIG. 8.—X-ray surface brightness profile in the 0.42–2.48 keV band from the combined HRI + PSPC data with 1 σ error bars.

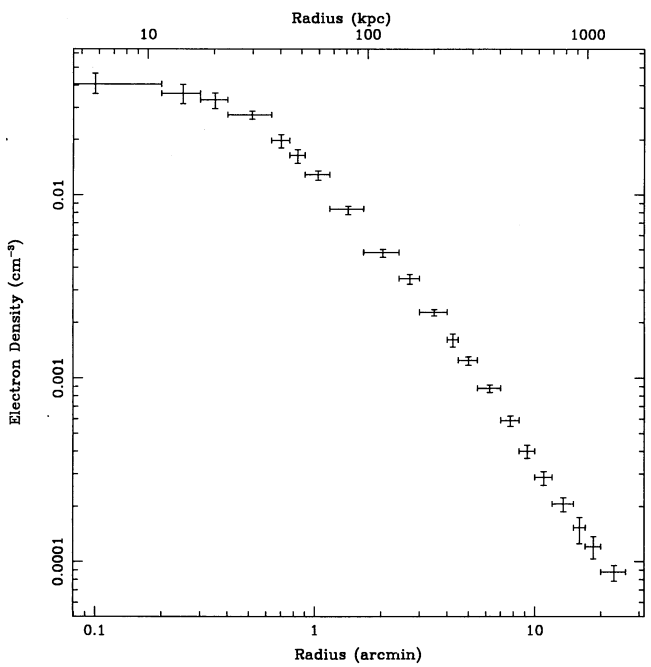

FIG. 9.—Deprojected electron density profile for 2A 0335+096. The error bars give the 10 and 90 percentile values from 1000 Monte Carlo simulations. Many of the bins in the surface brightness profile were combined in order to ensure a monotonically decreasing density profile.

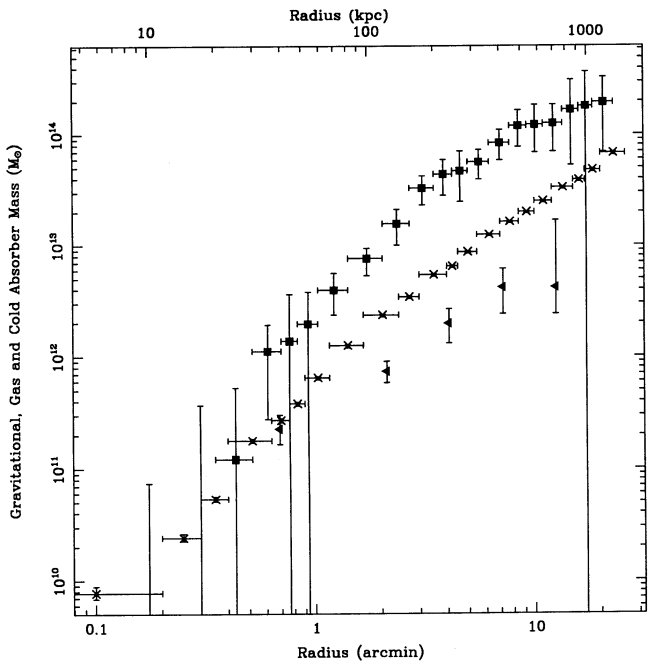

FIG. 10.—Profiles of the accumulated gas mass (*crosses*), accumulated gravitational mass (*filled boxes*) and accumulated cold absorber mass (*filled triangles*) in 2A 0335+096. The error bars for the gas and gravitational mass are the 10 and 90 percentile values from 1000 Monte Carlo simulations.

tating mass in the system within radius r is given by

$$M(<r) = -\frac{rkT(r)}{\mu m_{\rm H} G}\left[\frac{d\ln\rho(r)}{d\ln r} + \frac{d\ln T(r)}{d\ln r}\right]. \quad (3)$$

Equation 3 was applied to the derived density and temperature profiles in 2A 0335+096. It was necessary to combine some of the bins in order to ensure a monotonically increasing gravitational mass profile. The accumulated gas and gravitational mass profiles are shown in Figure 10. Statistical errors on these quantities are not easily assigned since the errors in the emissivities at different radii are correlated by the deprojection. Therefore, a Monte Carlo technique (Arnaud 1988) has been adopted to assign errors to all quantities derived from the emissivity. A simulated surface brightness profile was generated by randomly selecting an X-ray count value for each radial bin from a Poisson distribution with a mean equal to the number of counts in the original data for that bin. A simulated temperature profile was also created by randomly selecting temperature values for the innermost annulus and the outer four annuli combined from Gaussian distributions with means equal to the temperature values derived from the original data for these two regions. These two profiles were used to generate simulated electron density, gas mass, gravitational mass, and cooling rate profiles. This procedure was repeated 1000 times and errors were chosen to be the 10 and 90 percentile values from the 1000 simulations. The gas mass (the lower profile in Fig. 10) contributes 21% of the total gravitating mass (upper profile) at a radius of 70 kpc, and increases to 30% at a radius of 1.2 Mpc.

The integrated cooling time in the gas was calculated at each radius for which the deprojection gave a value of the gas density. The heavy element abundances were fixed at 40% of solar. The cooling radius r_c is defined as the radius at which the integrated cooling time is equal to the age of the cluster, for which a value 10^{10} yr was assumed. From the derived density profile, we found that the cooling radius was $r_c = 166^{+28}_{-18}$ kpc. The central ($\lesssim 5.75$ kpc) values for the electron density, pressure, and integrated cooling time are listed in Table 3, along with several other relevant cluster data derived in this paper.

7. COOLING MASS DEPOSITION RATE

We have determined the cooling rate profile using the technique described in Arnaud (1988). The X-ray emissivity deprojection (§ 6) is used to determine the X-ray luminosity generated in each spherical shell in the deprojection. The luminosity in each shell is assumed to result from the release of gravitational and thermal energy from gas cooling out of the flow in that shell, and from gas that flows through the shell but does not cool below X-ray emitting temperatures. The rate at which mass drops out of the flow in shell i, $\Delta\dot{M}_i$, is given by (Fabian et al. 1985)

$$\Delta\dot{M}_i = \frac{\Delta L_i - \dot{M}_{i-1}(\Delta H_i + \Delta\phi_i)}{H_i + f_i\Delta\phi_i}, \quad (4)$$

where ΔL_i is the change in bolometric luminosity across shell i, $\dot{M}_{i-1}$ is the rate at which mass passes through shell i but does not cool out of the flow, H_i and ΔH_i are the enthalpy per unit mass ($=5kT(r)/2\mu m_{\rm H}$) and the change in the enthalpy per unit mass in shell i, $\Delta\phi_i$ is the change in potential across shell i, and f_i is a geometrical factor that accounts for the fact that mass cools out of the flow in a volume-averaged manner.

The total integrated cooling rate at a distance r is then equal to the sum of the mass dropping out of the flow in all the shells at radii less than r_n:

$$\dot{M}(<r_n) = \sum_{i=1}^{n}\Delta\dot{M}(r_i). \quad (5)$$

The resulting integrated cooling rate profile is shown in Figure 11, along with the 10 and 90 percentile values from the 1000 Monte Carlo simulations.

Many previous studies of clusters have found cooling rates that increase as $\dot{M} \propto r$ out to the cooling radius (see, e.g., Fabian et al. 1981; Arnaud 1988). However, the cooling rate of 2A 0335+096 clearly peaks at a value of 400 $M_\odot$ yr^{-1} around 60 kpc, where the integrated cooling time is $\sim 2 \times 10^9$ yr, and then levels off. Similar results were found for several clusters by Edge, Stewart, & Fabian (1992) and for the NGC 5044 group of galaxies by David et al. (1994). They concluded that the radius at which the cooling flow became inhomogeneous (gas existing over a range of densities at a given radius) was coincident with the maximum in the temperature profile. It was at this point that radiative cooling began to dominate over gravi-

TABLE 3

CLUSTER PROPERTIES

Property	Value
Global temperature (keV)	3.1
Central electron density (cm^{-3})	$4.1 \times 10^{-2}\ h_{50}^{1/2}$
Central pressure (K cm^{-3})	$8.1 \times 10^{5}\ h_{50}^{1/2}$
Gravitating mass within 1.2 Mpc ($M_\odot$)	$1.9 \times 10^{14}\ h_{50}^{-1}$
Gas mass within 1.2 Mpc ($M_\odot$)	$5.8 \times 10^{13}\ h_{50}^{-5/2}$
Central cooling time (yr)	$6.5 \times 10^{8}\ h_{50}^{-1/2}$
Cooling radius (kpc)	166
Cooling rate ($M_\odot$ yr^{-1})	$400\ h_{50}^{-2}$

NOTE.—Here $h_{50} = H_0/50$ km s^{-1} Mpc^{-1}.

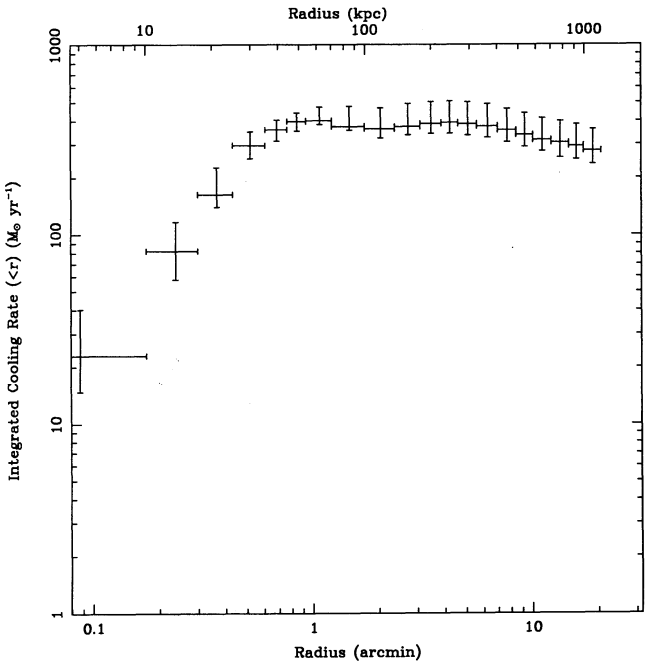

FIG. 11.—Integrated cooling rate profile for the cluster. The error bars are the 10 and 90 percentile values from 1000 Monte Carlo simulations.

tational heating. We cannot test that suggestion here since the smearing of energy due to the XRT and PSPC point spread function does not allow us to divide the inner 60 kpc into multiple bins as was done for the NGC 5044 group.

Interestingly, we found that if a constant 3.1 keV temperature profile was used throughout the procedure, a cooling rate profile that was roughly proportional to radius out to the cooling radius was obtained. Since a single global temperature value was all that was available in previous *Einstein* and *EXOSAT* studies of clusters, it is possible that the $\dot{M} \propto r$ relation derived in some of these studies might be an artifact of using a single temperature or a model for the potential to derive the temperature gradient.

8. DISCUSSION

Spectral fitting of the inner regions of the 2A 0335+096 cluster of galaxies confirms the presence of a low-temperature component of the X-ray emitting gas, a strong indication that a cooling flow is present in this cluster. Evidence of X-ray absorbing matter intrinsic to the cluster was also found. Although the need for cold, absorbing matter to explain the deficit of soft X-rays in the cores of cooling flow clusters is well-documented (White et al. 1991; Allen et al. 1993; Allen & Fabian 1994), its existence is still somewhat controversial as the bulk of this material is presently undetectable at any wavelength other than in the X-ray band. Nevertheless, absorption due to a significant amount of matter within clusters provides the most reasonable means of explaining the deficit of soft X-rays in the spectra of some cooling flow regions.

From the spectral fitting of the inner two annuli in § 4, a mass of $7.4 \times 10^{11}\ M_{\odot}$ is inferred for the absorbing matter within a radius of 170 kpc (the absorbing mass in an annulus is $m_{\rm H} \Delta N_{\rm H} A$, where A is the cross-sectional area of the annulus). At a cooling rate of $400\ M_{\odot}\ {\rm yr}^{-1}$, this mass could be deposited by the cooling flow in about 2×10^9 yr, which is also (coincidentally?) the cooling time at 60 kpc where the flow appears to become inhomogeneous. An absorbing mass of $3.4 \times 10^{12}\ M_{\odot}$ is inferred for the third and fourth annuli (170–520 kpc). A radial profile of the accumulated mass of the cold absorber is shown in Figure 10. The intrinsic absorber has a total mass of $4.2 \times 10^{12}\ M_{\odot}$, which corresponds to the total cooled mass accumulated in about 10^{10} yr at a cooling rate of $400\ M_{\odot}\ {\rm yr}^{-1}$. However, this absorber is apparently distributed over a region that is considerably larger than the cooling radius, and an order of magnitude larger than the radius within which $\dot{M}(r)$ decreases. Thus, the absorber occurs over a much larger volume than the region where gas is cooling today. Assuming that the absorber is the product of the X-ray cooling gas, it is not apparent how the absorbing matter was transported out half a megaparsec from the center of the cluster. A similar radial trend in the absorption profile was found in the cluster Abell 478, with evidence for excess absorption present out to a radius of 1 Mpc (White et al. 1994).

One idea is that the cluster may have undergone a recent merger and the merging process may have redistributed the absorbing matter in the cooling flow region to larger radii. Although a galactic merger is apparently occurring between the central D galaxy and a companion galaxy 6″ to the northwest (Sarazin et al. 1992), the X-ray contours at large radii do not show any evidence of a recent disturbance (Fig. 1). This would seem to rule out the possibility of a very recent merger. However, if the cluster had undergone a merger in the distant past, the X-ray emitting gas would have had time to settle after a few sound crossing times (few $\times 10^9$ yr) and the X-ray contours would appear smooth and regular.

Assuming that a subcluster merger has occurred in the distant past in this cluster, there are two ways in which the absorbing material could have been redistributed. First, cold absorbing material already present in each subcluster mixed and distributed itself at large radii following the merger. One might expect such an event to redistribute material preferentially in the orbital plane of the merger. To test for this possibility, the azimuthal dependency of the intrinsic absorption at large radii was determined by performing spectral fits on four wedge-shaped regions, each with an inner radius of 166 kpc (the cooling radius) and outer radius of 520 kpc (the outer edge of the fourth annulus) and each 90 degrees in angular extent. Again, a variable absorption model (model 2) was used with the metallicity fixed at 40%. Although the amount of excess absorption was comparable in all four regions, the error bars associated with the excess column density were so large as to render the results meaningless for this particular observation. Better statistics are necessary in order to address this issue. Second, it might be that hot gas already present in each subcluster mixed and distributed itself at large radii following the merger, resulting in a bimodal density distribution of hot gas. That is, both high- and low-density parcels of gas existed simultaneously at all radii. The dense parcels cooled quickly and were deposited in the form of cold gas clouds, even at large radii. Over time, the dense parcels were eventually depleted and condensed into cold clouds at large radii, leaving only gas that was at too low a density to cool out of the flow. As a result, the flow became more homogeneous, and mass deposition was halted except at small radii. Unfortunately, this hypothesis is difficult to test.

A merger model might account for the fact that the cooling rate profile peaks well inside the cooling radius. It has often been argued that a major subcluster merger will disrupt a

cluster cooling flow (see, e.g., McGlynn & Fabian 1984). Following the merger a cooling flow should be reestablished once the hot gas has settled and reached hydrostatic equilibrium. Only gas with a cooling time less than the time since the merger occurred would cool out of the flow. The cooling radius for 2A 0335+096 was determined by assuming the cluster's age was 10^{10} yr. If a major subcluster merger has occurred and disrupted the previously existing cooling flow, the cooling radius for the reestablished cooling flow would be considerably smaller, as gas at larger radii has not yet had time to cool. As noted in § 7 above, the cooling time in 2A 0335+096 at 60 kpc (where the cooling rate profile flattens) is about 2×10^9 yr. If a major subcluster did occur several billion years ago, we might be seeing the reestablished cooling flow in this cluster.

The total gravitating mass within 1.2 Mpc is $1.9 \times 10^{14} M_\odot$. Hot gas comprises 30% of this mass, and the ratio of gas to gravitational mass increases with radius. Our measurements set a lower limit on the baryon fraction within the cluster, as we have not included the mass of the individual galaxies. Comparable baryon fractions have been found for many other clusters and groups (see, e.g., Briel et al. 1992; Allen & Fabian 1994; David et al. 1994). These results conflict with primordial nucleosynthesis calculations and inflation, which predict an upper limit of 0.06 for the baryon fraction in an $\Omega = 1$ universe (see, e.g., Walker et al. 1991).

9. CONCLUSIONS

Observations of the cluster 2A 0335+096 with the *ROSAT* PSPC and HRI confirm the existence of a cooling flow in this cluster. An ambient temperature of 3.1 keV was found for the outer regions. The temperature was found to decrease to 1.5 keV at a radius of 40 kpc. We present electron density and gravitational and gas mass profiles out to a radius of 1.2 Mpc. Using the spectrally determined temperature profile, a cooling rate of 400 $M_\odot$ yr^{-1} was derived from the deprojection of the surface brightness profile. This value is in good agreement with the cooling rate obtained from spectral fitting of the inner 166 kpc, the cooling radius. The cooling rate profile peaks around 60 kpc, well within the cooling radius. This suggests that a large portion of the cooling flow is homogeneous, in contrast to studies of other clusters (see, e.g., Fabian et al. 1981). We also find that a cooling rate proportional to radius out to the cooling radius is obtained if a constant temperature profile is used in our procedure instead of the observed temperature profile.

A total gravitating mass of $1.9 \times 10^{14} M_\odot$ was found within 1.2 Mpc, of which 30% is hot, X-ray emitting gas.

We find evidence for absorption in excess of that due to the measured Galactic column density, which is concentrated to the core of the cluster. The absorption column density decreases radially out to a radius of 0.5 Mpc. The total mass implied for this absorbing matter is approximately $4.2 \times 10^{12} M_\odot$, and is presumably in the form of cold, dense clouds. The mass of this absorber corresponds reasonably to the mass expected to cool out of the cooling flow in a reasonable cluster age of approximately 10^{10} yr. However, the absorber extends further than the present cooling radius, and much further than the radius (60 kpc) at which the cooling rate flattens and the mass deposition appears to stop at present. It is possible that the gas was cooling at larger radii in the past as a result of a subcluster merger.

J. A. I. thanks Zhenping Huang, Robert O'Connell, and Mark Whittle for useful conversations, Jeffrey Breen for information regarding XSPEC, and an anonymous referee for useful comments and suggestions. C. L. S. thanks Stefi Baum, Brian McNamara, and Chris O'Dea for useful conversations and other help. We would like to thank Ralph Bohlin of the Space Telescope Science Institute for kindly providing a digitized version of the *Hubble Space Telescope* Guide Star Catalog field of this region. C. L. S. was supported in part by NASA Astrophysical Theory Program grant NAGW-2376, and J. A. I and C. L. S. were supported by NASA *ROSAT* grants NAG 5-1577 and NAG 5-1891.

REFERENCES

Allen, S. W., & Fabian, A. C. 1994, MNRAS, 269, 409
Allen, S. W., Fabian, A. C., Johnstone, R. M., White, D. A., Daines, S. J., Edge, A. C., & Stewart, G. C. 1993, MNRAS, 262, 901
Arnaud, K. A. 1988, in Cooling Flows in Clusters & Galaxies, ed. A. C. Fabian (Dordrecht: Kluwer), 31
Briel, U. G., Henry, J. P., & Böhringer, H. 1992, A&A, 259, L31
David, L. P., Harnden, F. R., Kearns, K. E., & Zombeck, M. V. 1992, The *ROSAT* High Resolution Imager (HRI) (Cambridge: Smithsonian Astrophys. Obs.)
David, L. P., Jones, C., Forman, W., & Daines, S. J. 1994, ApJ, 428, 544
Edge, A. C., Stewart, G. C., & Fabian, A. C. 1992, MNRAS, 258, 177
Fabian, A. C. 1994, ARA&A, 32, 277
Fabian, A. C., Arnaud, K. A., Nulsen, P. E. J., Watson, M. G., & Mushotzky, R. F. 1985, MNRAS, 216, 923
Fabian, A. C., Hu, E. M., Cowie, L. L., & Grindlay, J. 1981, ApJ, 248, 47
Fabian, A. C., Nulsen, P. E. J., & Canizares, C. R. 1982, MNRAS, 201, 933
Hasinger, G., Turner, T. J., George, I. M., & Boese, G. 1992, GSFC OGIP Calibration Memo CAL/ROS/92-001, NASA
Huang, Z., & Sarazin, C. L. 1996, in preparation
Jedrzejewski, R. I. 1987, MNRAS, 226, 747
Kaastra, J. S. 1992, An X-Ray Spectral Code for Optically Thin Plasmas (Internal SRON-Leiden Report, updated version 2.0)
Lasker, B. M., et al. 1988, ApJS, 68, 1
McGlynn, T. A., & Fabian, A. C. 1984, MNRAS, 208, 709
Mitchell, R. J., Culhane, J. L., Davison, P. J. N., & Ives, J. C. 1976, MNRAS, 175, 29P
Morrison, R., & McCammon, D. 1983, ApJ, 270, 119
Mushotzky, R. F., & Szymkowiak, A. E. 1988, in Cooling Flows in Clusters & Galaxies, ed. A. C. Fabian (Dordrecht: Kluwer), 53
O'Connell, R. W., & McNamara, B. R. 1989, AJ, 98, 180
Plucinsky, P. P., Snowden, S. L., Briel, U. G., Hasinger, G., & Pfeffermann, E. 1993, ApJ, 418, 519
Raymond, J. C., & Smith, B. W. 1977, ApJS, 35, 419
Romanishin, W., & Hintzen, P. 1988, ApJ, 324, L17
Sarazin, C. L., Baum, S. A., & O'Dea, C. P. 1995, ApJ, 451, 125
Sarazin, C. L., & O'Connell, R. W. 1983, ApJ, 268, 552
Sarazin, C. L., O'Connell, R. W., & McNamara, B. R. 1992, ApJ, 389, L59
Serlemitsos, P. J., Smith, B. W., Boldt, E. A., Holt, S. S., & Swank, J. H. 1977, ApJ, 211, L63
Silverman, B. W. 1986, Density Estimation for Statistics & Data Analysis (New York: Chapman & Hall)
Singh, K. P., Westergaard, N. J., & Schnopper, H. W. 1986, ApJ, 308, L51
———. 1988, ApJ, 331, 672
Stark, A. A., Gammie, C. F., Wilson, R. W., Bally, J., Linke, R. A., Heiles, C., & Hurwitz, M. 1992, ApJS, 79, 77
Vaiana, G. S. 1990, in Imaging X-ray Astronomy: A Decade of *Einstein Observatory* Achievements, ed. M. Elvis (Cambridge: Cambridge Univ. Press), 61
Walker, T. P., Steigman, G., Schramm, D. N., Olive, K. A., & Kang, H. 1991, ApJ, 376, 51
White, D. A., Fabian, A. C., Allen, S. W., Edge, A. C., Crawford, C. S., Johnstone, R. M., Stewart, G. C., & Voges, W. 1994, MNRAS, 269, 589
White, D. A., Fabian, A. C., Johnstone, R. M., Mushotzky, R. F., & Arnaud, K. A. 1991, MNRAS, 252, 72
White, S. D. M., Navarro, J. F., Evrard, A. E., & Frenk, C. S. 1993, Nature, 366, 429